AIAA JOURNAL
Vol. 30, No. 9, September 1992

Experiments on the Structure of an Annular Compressible Reacting Shear Layer

R. S. Barlow*
Sandia National Laboratories, Livermore, California 94551
D. C. Fourguette†
California Institute of Technology, Pasadena, California 91125
M. G. Mungal‡
Stanford University, Stanford, California 94395
and
R. W. Dibble§
University of California, Berkeley, Berkeley, California 94720

An axisymmetric burner for the study of compressible reacting shear layers is described, and the ranges of its operating parameters are analyzed. This burner has a central supersonic freejet of resistively heated air, surrounded by a low-speed co-flow of fuel-rich H_2-air combustion products. Planar laser-induced fluorescence imaging of OH is used to visualize the structure of the annular reacting shear layer in the near field of the jet. Images from two cases with convective Mach numbers of 0.11 and 0.41 are presented and discussed in terms of previously reported results for nonreacting compressible shear layers. Observed effects of compressibility on the structure and growth rate of the reacting annular shear layer are similar to effects reported in nonreacting flows. Results from a compressible "lifted" flame and from the reaction zone at the boundary of an underexpanded jet are presented.

Introduction

In supersonic combustion one expects the structure and growth rate of a turbulent shear layer to be influenced by compressibility and heat release. Dimotakis[1] has reviewed much of the data on the separate effects of compressibility and heat release on shear layer structure. It has been well established, experimentally, that compressibility reduces the growth rate of nonreacting turbulent free shear layers.[2-7] The convective Mach number[2,8] has been shown to be a parameter that collapses much of the available data on compressible shear layer growth. Experiments have also shown that turbulence levels and Reynolds stresses decrease as the convective Mach number increases.[5,9] Numerical studies[10-12] have predicted increased stability and reduced growth rates when the velocity difference between the two mixing streams is comparable to or greater than the speed of sound. In particular, the two-dimensional Kelvin-Helmholz instability, which leads to the large-scale spanwise vortical structures observed by Brown and Roshko[13] and others, becomes less important. Three-dimensional instabilities become dominant, producing oblique structures in the shear layer, as reported by Sandham and Reynolds.[14] The influence of these oblique structures on entrainment of fluid into the layer has been studied numerically by Chen.[15] Conserved scalar statistics from these simulations suggest that fluid is engulfed into the layer in several small steps, rather than in one continuous motion. The increased three dimensionality predicted by the numerical studies of nonreacting planar shear layers has been confirmed by the experiments of Fourguette et al.[16] and Clemens and Mungal.[17]

For low-speed, incompressible turbulent shear layers, experimental[18,19] and computational[20,21] studies have shown that heat release from chemical reactions within the layer causes a small reduction in the growth rate. The combined effect of compressibility and heat release on the turbulent mixing process is an important research area in the context of supersonic combustion. Shin and Ferziger[22] have investigated the stability of a compressible reacting mixing layer. However, few experimental studies on supersonic combustion have been completed, and much remains to be learned about the combined effects of compressibility and heat release on the structure and growth of turbulent mixing layers.

In addition to the fluid dynamic effects of compressibility and heat release on the structure of compressible reacting flows, the effects of competition between high turbulent mixing rates and finite chemical reaction rates in supersonic flames (the effects of a low Damköhler number) are an important issue. Magre and Dibble[23] and Barlow et al.[24] have quantified the effects Damköhler number on temperature depression and OH superequilibrium in subsonic hydrogen jet diffusion flames. Mungal and Frieler[25] investigated the influence of the Damköhler number on product formation rates in a subsonic planar turbulent reacting shear layer. Results of these studies have shown that finite-rate chemistry effects correlate well with a Damköhler number based on the local, large-scale strain rate or mixing time. Kerstein[26] has investigated mixing and reaction in turbulent shear layers using a linear eddy model and has reported that product formation scales with a Damköhler number based on the large eddy time. However, again, there is little experimental data available on the effects of finite-rate chemistry in supersonic combustion environments.

This paper reports the first results of an experimental program to investigate the effects of the convective Mach number and of the Damköhler number (ratio of chemical reaction rate

Presented as Paper 91-0376 at the AIAA 29th Aerospace Sciences Meeting, Reno, NV, Jan. 7-10, 1991; received May 13, 1991; revision received Nov. 25, 1991; accepted for publication Jan. 7, 1992.

*Senior Member of Technical Staff, Combustion Research Facility. Member AIAA.
†Research Fellow, Graduate Aeronautics Laboratory, Member AIAA.
‡Associate Professor, Mechanical Engineering Department. Member AIAA.
§Associate Professor, Mechanical Engineering Department.

to turbulent mixing rate) on the structure of reacting turbulent shear layers. The burner developed for the present study consists of an unconfined supersonic round jet of heated air, surrounded by a low-speed co-flow of fuel-rich combustion products from a flat flame of premixed hydrogen and air. In the near field of the jet there is a reacting mixing layer between the supersonic potential core of the jet and the co-flowing gas. Planar laser-induced fluorescence (PLIF) imaging of OH is used to visualize the structure of this annular reaction zone.

In the following sections the design of the burner is outlined, and the ranges of certain operating parameters are analyzed. Some aspects of the practical operation of the burner are discussed, and the results of PLIF imaging experiments are presented for a selected set of conditions that begin to illuminate the effects of the convective Mach number and the Damköhler number in compressible reacting shear layers.

Axisymmetric Burner Design

The choice of an axisymmetric burner represents an extension of ongoing experiments at Sandia on the structure of subsonic turbulent hydrogen jet flames[23,24,27] and on the structure of compressible nonreacting jets.[16,28] This geometry allows application of laser diagnostics without the complication of wall effects and windows. The axisymmetric geometry also allows for a relatively simple facility that utilizes existing flow capacities for compressed air, hydrogen, and exhaust. The burner, shown in Fig. 1, consists of an interchangeable central nozzle surrounded by a large-diameter, premixed, flat-flame burner. This device can be operated with either air or hydrogen as the central, high-speed jet fluid. By using air in the central jet, the hydrogen flow requirement of the device and the heat load to the exhaust system are reduced significantly for a given nozzle diameter. The flame length is also reduced substantially because the flame ends when entrainment and combustion of the flat-flame products is complete.

Temperature-controlled process gas heaters are used to resistively heat the air for the central jet to a maximum stagnation temperature of 870 K. The house compressor system delivers air at sufficient pressure to operate the central jet up to an exit Mach number of 2. In the present experiments a Mach 1.5 converging-diverging nozzle and a simple converging nozzle (for subsonic cases) are used. The throat diameter of each nozzle is 8 mm, which represents a compromise between the capacity of the flow facilities for continuous operation and the desire to obtain the largest practical flowfield dimensions. The temperature of the air flow is measured using

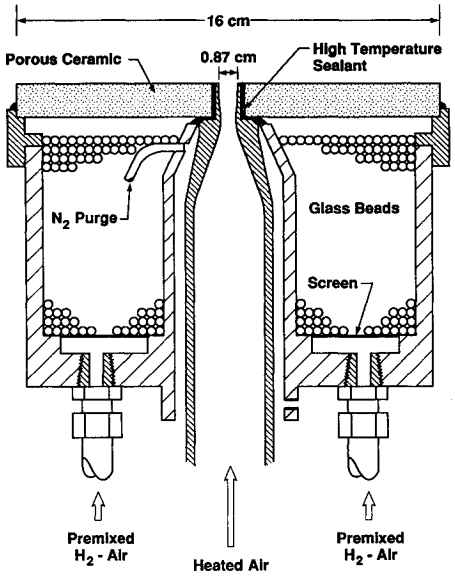

Fig. 1 Burner design for axisymmetric, supersonic combustion experiments.

a thermocouple located near the centerline of the air plenum below the nozzle. Pressure is also measured in the air plenum. The Mach number in this air plenum is ~0.1, and the measured temperature and pressure are taken as stagnation conditions.

The flat-flame burner that surrounds the central nozzle uses a porous ceramic disk to stabilize a premixed hydrogen-air flame. The top surface of the ceramic is flush with the nozzle exit. The inner plenum wall of the flat flame burner is separated from the hot central tube by a gap that is loosely packed with ceramic insulation and purged with a low flow rate of nitrogen. Flow rates of air and hydrogen supplied to the premixed flame are measured using sonic nozzles. With air as the central jet fluid, the premixed flame is operated fuel-rich, and the excess H_2 reacts with the central air at the boundary of the jet. In the near field of the jet, where there is still a potential core, reaction occurs in an annular shear layer between the high-speed air and the low-speed co-flowing gases. This reacting turbulent shear layer is the focus of the present study.

The flat-flame burner can be operated in a standby mode by adding a small flow of methane to the hydrogen-air mixture. The methane causes the fuel-rich premixed flame to lift off the ceramic surface, allowing the ceramic to stay cool between image acquisition events. The flame remains attached at the outer rim of the ceramic disk, where the premixed flame meets the diffusion flame that forms between the fuel-rich mixture and the ambient air. To obtain the PLIF images, the methane is turned off for a few seconds, causing the premixed H_2-air flame to burn at the ceramic surface.

Operating Parameters of the Burner

The burner described in the preceding section allows for a variation of the Mach number of the central air jet (by changing nozzles), the temperature of the air jet, and the temperature and composition of the outer, low-speed flow. In the following analysis, relationships for nonreacting planar shear layers are used to estimate the range of convective Mach numbers that can be investigated using this burner. In addition, the width of the shear layer in the near field of the jet and the equivalence ratio of the mixed fluid within the shear layer are estimated from relationships for nonreacting flows.

Relationships for planar shear layers are used because there is a significant body of experimental for planar shear layers and comparable correlations for annular shear layers could not be found. One might expect some structural differences between planar and annular shear layers, due to the azimuthal instability modes that exist for the annular case. Tam and Hu[29] have identified three families of instability waves in high-speed jets. Their results suggest that only the Kelvin-Helmholtz instability would be active in the present subsonic and low supersonic flows. However, experiments have shown that azimuthal structure can appear quite early in the development of the annular shear layer in the near field of a jet (see, for example, Fig. 12 of Fourguette et al.[16] and Fig. 10 of Samimy et al.[30]).

The convective velocity U_c is determined by matching isentropic recovery pressures of fluids from the two streams meeting at an interface within the shear layer (a stagnation point in the convective frame of reference), such that

$$\left[1+\frac{\gamma_1-1}{2}\left(\frac{U_1-U_c}{a_1}\right)^2\right]^{\gamma_1/(\gamma_1-1)} = \left[1+\frac{\gamma_2-1}{2}\left(\frac{U_c-U_2}{a_2}\right)^2\right]^{\gamma_2/(\gamma_2-1)} \quad (1)$$

where U, a, and γ are the velocity, speed of sound, and ratio of specific heats of the two streams, respectively, and the subscripts 1 and 2 refer to the high-speed side and low-speed

side, respectively. Convective Mach numbers are then calculated as

$$M_{c,1}=\frac{(U_1-U_c)}{a_1}, \qquad M_{c,2}=\frac{(U_c-U_2)}{a_1} \tag{2}$$

To evaluate the operating range of the convective Mach number for the present burner, we first consider the properties of the product gas stream above the premixed flat flame. Figure 2 shows the variation with equivalence ratio ϕ_2 of the adiabatic equilibrium properties of this low-speed stream. (There is some heat loss to the burner surface; however, the adiabatic assumption is sufficient for estimating the range of operating parameters.) For fuel-rich hydrogen-air combustion, molecular weight decreases rapidly with increasing equivalence ratio. The decrease in molecular weight offsets the decrease in temperature, such that the density ρ_2 and the speed of sound a_2 of the low-speed stream are relatively weak functions of ϕ_2. Consequently, the convective Mach number of the annular shear layer in the near field of the jet is insensitive to ϕ_2 and depends primarily on the properties of the central air jet.

Figure 3 shows convective Mach number $M_{c,1}$ vs the stagnation temperature of the air stream for three values of the air-side Mach number ($M_1=1.5$, 1.7, and 2.0) and an equivalence ratio of $\phi_2=5$ in the low-speed stream. The convective Mach number increases as the temperature and/or the Mach number of the high-speed air increase. With the present burner design, we can obtain convective Mach numbers up to ~ 0.54 when air is the central jet fluid. Convective Mach numbers up to 0.80 could be reached by using a mixture of 20% oxygen in helium as the central jet fluid.

The spreading rate of a planar incompressible turbulent mixing layer, based on a correlation of experimental measurements of the visual thickness, is given by Papamoschou[3] as

$$\frac{\delta_i}{x}=\frac{0.17(1-r)(1+\sqrt{s})}{1+r\sqrt{s}} \tag{3}$$

where $r=U_2/U_1$ is the velocity ratio and $s=\rho_2/\rho_1$ is the density ratio for the two streams. The ratio of compressible to incompressible shear layer growth rates can be estimated using

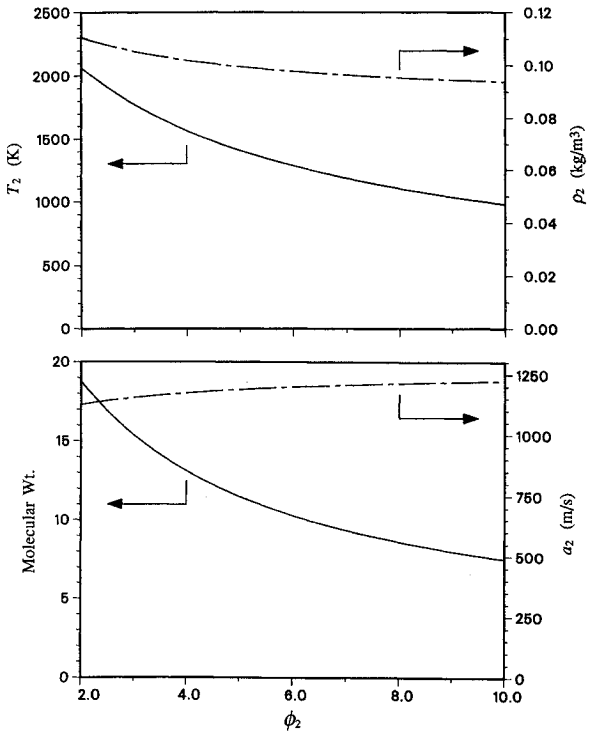

Fig. 2 Properties of the H_2-air products above the flat flame as functions of the equivalence ratio ϕ_2 assuming adiabatic equilibrium.

the following expression from Dimotakis[1]:

$$\frac{\delta}{\delta_i}\cong(1-f_\infty)e^{-3M_{c,1}^2}+f_\infty, \qquad f_\infty=0.2 \tag{4}$$

Equations (3) and (4) are combined to estimate the shear layer growth rate in the absence of heat release effects. As for the convective Mach number, the estimated growth rate δ/x is relatively insensitive to ϕ_2 and depends primarily on the Mach number and the temperature of the high-speed airstream. Average widths of OH fluorescence images of the reacting shear layer are compared later with estimates of the shear layer width based on Eqs. (3) and (4).

The volumetric entrainment ratio E_v (high-speed fluid volume divided by low-speed fluid volume) is important because it determines the stoichiometry of the mixed fluid within the shear layer. This entrainment ratio for incompressible shear layers can be expressed as[1]

$$E_v\cong s^{1/2}[1+0.68(1-r)/(1+r)] \tag{5}$$

Dimotakis[1] has suggested a possible modification to Eq. (5) to account for the effect of compressibility on the entrainment ratio. However, in the absence of experimental data on the entrainment ratio for compressible shear layers, we will use the incompressible form shown earlier. The equivalence ratio ϕ_s of the mixed fluid within the shear layer is calculated from the volumetric entrainment ratio, the density ratio, and the mass fraction of H_2 in the low-speed stream:

$$\phi_s\cong\frac{(s/E_v)Y_{H2,2}}{0.0292} \tag{6}$$

where 0.0292 is the stoichiometric H_2-air mass ratio. Products of combustion other than the excess molecular hydrogen in the low-speed stream are treated as diluents for the purpose of this calculation.

Figure 4 shows ϕ_s vs ϕ_2 with the stagnation temperature of the high-speed airstream as a parameter for the case where the Mach number of the airstream is 1.5. The important result here is that the burner can be operated at conditions where the equivalence ratio of the mixed fluid in the shear layer is near unity. This has two useful consequences. First, we can expect OH fluorescence to be a good qualitative marker of the mixed (and reacted) shear layer fluid because the OH radical concentration in hydrogen flames peaks near the stoichiometric condition, and high OH concentrations occur over a relatively broad range of the equivalence ratio. In turbulent diffusion flames the stoichiometric contour is often separated from the center of the shear layer. This separation of the reaction zone from the turbulent shear layer has been observed in numerous experiments investigating the near field structure of turbulent jet diffusion flames. The same condition can be expected to

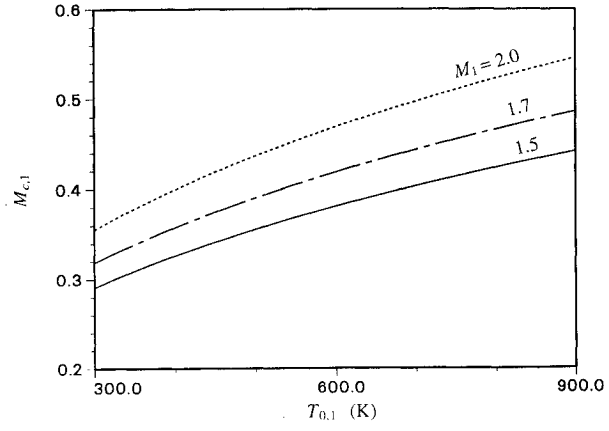

Fig. 3 Convective Mach number $M_{c,1}$ vs stagnation temperature $T_{0,1}$ of the air for jet Mach numbers of $M_1=1.5$, 1.7, and 2.0, with an equivalence ratio in the outer low-speed flow of $\phi_2=5$.

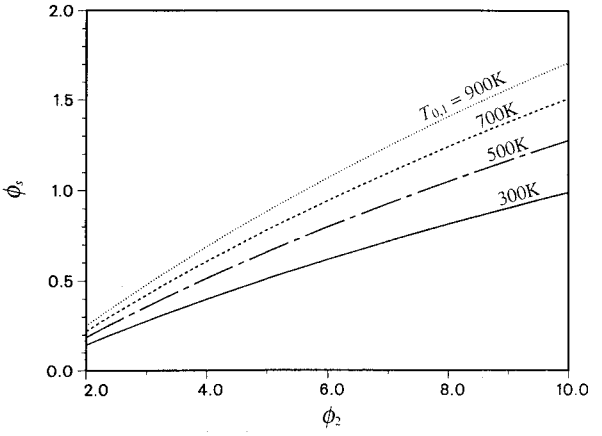

Fig. 4 Equivalence ratio ϕ_s of the mixed fluid in the shear layer vs ϕ_2 for a Mach 1.5 jet with stagnation temperatures of $T_{0,1}$ = 300, 500, 700, and 900 K.

prevail for non-premixed H_2-air combustion in turbulent shear layers when the fuel side is pure hydrogen. In such flames OH fluorescence may be a good marker of the reaction zone, but OH images may not provide a good indication of the structure of the shear layer. The second useful consequence of the results in Fig. 4 is that the equivalence ratio ϕ_s can be varied from lean to rich to investigate the effects of the mixed fluid stoichiometry on the structure of the shear layer. Because the convective Mach number is relatively insensitive to ϕ_2, this variation of the mixed fluid equivalence ratio can be carried out with the convective Mach number being held nearly constant.

Apparatus and Procedures for PLIF Imaging

The apparatus for PLIF imaging of OH is shown schematically in Fig. 5. The 532-nm output of a pulsed, doubled Nd:YAG laser pumps a tunable dye laser. The dye laser beam is doubled into the uv to excite the $A^2\Sigma - X^2\Pi(1\text{-}0)$ $Q_1(8)$ transition of OH near 283 nm. The uv beam is formed into a vertical sheet ~3 cm high and directed through the centerline of the jet. Fluorescence is imaged using reflective optics onto an intensified Photometrics CCD array. An interference filter (313 nm center wavelength, 10 nm width) is mounted in front of the image intensifier and transmits (1-1) fluorescence. Images are acquired onto a computer using software developed by Long.[31] The width of the laser sheet is ~150 μ near the center of the image frame and remains below 200 μ across the portion of the flowfield that includes the reaction zone. This sheet width is not sufficient to resolve all the scales in the flow. However, this limitation on spatial resolution is not a significant issue for the present exploratory work because we are primarily interested in characterizing the operating parameters of the burner and investigating the effects of compressibility on the structure of reacting shear layers at the largest scales.

The collection lens and CCD array are positioned to produce an object to image magnification of 0.64, so that a 13.7 mm × 20.5 mm region of the flow is imaged. This corresponds to a $1.7D \times 2.5D$ frame, where D is the exit diameter of the nozzle. Vertically and horizontally oriented images are obtained by rotating the camera. For both orientations the vertical center of the image is 38 mm, or 4.8 diam above the nozzle exit. Figure 6 shows the locations of the image frames relative to the nozzle. The vertical frame includes one side of the annular shear layer, with the low-speed fluid on the left side of the reaction zone and the high-speed air on the right. The horizontal frame includes the reaction zones on both sides of the annular shear layer and gives an indication of the relative widths of the reaction zone and the potential core of the jet.

Results and Discussion

When a Mach 1.5 nozzle was operating at the calculated matched pressure condition with static temperatures of ~500 K in the supersonic air jet, stable attached flames (annular

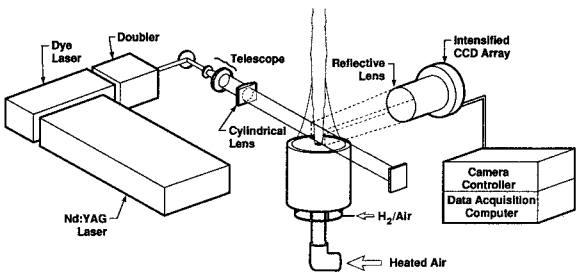

Fig. 5 Apparatus for PLIF imaging of OH in the supersonic reacting flows.

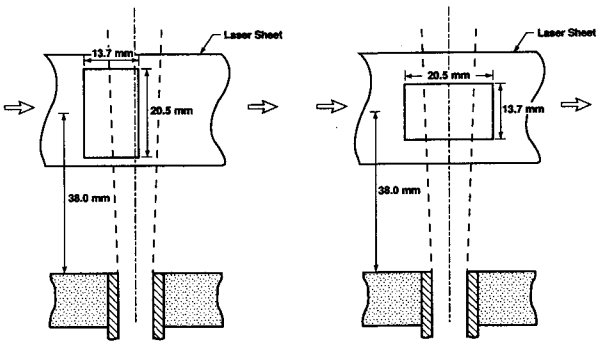

Fig. 6 Diagram of vertical and horizontal image orientations.

reaction zones) were observed for equivalence ratios up to $\phi_2 = 6.5$ in the premixed flat flame. For an equivalence ratio of $\phi_2 = 6.75$ in the low-speed stream, both visual observations and OH fluorescence images revealed a "lifted" flame structure, indicating that turbulent mixing rates exceeded chemical reaction rates in the early part of the shear layer. Based on these observations, sets of OH fluorescence images were obtained at four operating conditions. Flow parameters for the first three cases are summarized in Table 1. The values listed in Table 1 for the convective Mach number, the shear layer thickness, and the mixed-fluid equivalence ratio are based on Eqs. (1-6), the equations and correlations for nonreacting planar shear layers, and are included here as estimates of the properties of the reacting shear layer. Note that a local strain rate σ and time scale τ_{flow}, based on the velocity difference and the shear layer thickness at the center of the image frame (x = 38 mm), are tabulated. The Reynolds numbers in Table 1 are based on the velocity difference between the central jet and the co-flow, the calculated shear layer thickness, and the average of the viscosities of the two streams:

$$Re_\delta = \frac{(U_1 - U_2)\delta}{(\nu_1 + \nu_2)/2} \tag{7}$$

Here, the air viscosity ν_1 is evaluated at the calculated static temperature of the jet, and ν_2 is evaluated at the adiabatic equilibrium temperature for the listed H_2-air equivalence ratio.

Cases A and C are compressible flows with equivalence ratios on the low-speed side of $\phi_2 = 5.0$ and 6.75, respectively. Case B is an incompressible flow with a subsonic central jet issuing from a simple converging nozzle and with the same flat flame equivalence ratio as that in case A. The stagnation air temperature is lower in case B than in case A; thus, the static temperature on the high-speed side of the shear layer is nearly the same for the two cases. This facilitates direct comparison of the compressible and incompressible flows.

The fourth operating condition had an underexpanded central air jet. This case was considered to determine whether the shock structure of the underexpanded jet caused any observable change in the structure of the reacting shear layer. Because of the presence of shocks, however, there is not a simple way to calculate the properties of the high-speed side of the shear layer; thus, we have not included this case in Table 1.

Table 1 Experimental flow conditions[a]

Description	Case A supersonic, attached	Case B subsonic, attached	Case C supersonic, lifted
M_1	1.5	0.4	1.5
$T_{0,1}$, K	745.	522.	715.
$P_{0,1}$, kPa	379.	112.9	370.
T_1, K	514.	506.	493.
U_1, m/s	681.	180.	667.
a_1, m/s	454.	451.	445.
ν_1, m^2/s	3.95×10^{-5}	3.87×10^{-5}	3.70×10^{-5}
ϕ_2	5.0	5.0	6.75
(mol wt)$_2$	11.5	11.5	9.58
T_2, K	1400.	1400.	1210.
U_2, m/s	2.1	2.1	2.2
ν_2, m^2/s	4.65×10^{-4}	4.65×10^{-4}	4.17×10^{-4}
$Y_{H2,2}$	0.103	0.103	0.132
$M_{c,1}$	0.413	0.108	0.401
$r=U_2/U_1$	0.003	0.012	0.003
$s=\rho_2/\rho_1$	0.146	0.143	0.135
$\delta_{x=38\text{ mm}}$, mm	6.0	8.5	6.1
$\delta_{x=38\text{ mm}}$, s^{-1}	1.1×10^5	0.2×10^5	1.1×10^5
τ_{flow}, μs	9.1	50	9.1
E_ν	0.639	0.629	0.615
ϕ_s	0.81	0.80	0.99
Re_δ	16,400	6,000	17,900

[a]Properties of stream 2 are based on the assumption of adiabatic equilibrium above the premixed flame.

Differences Between Compressible and Incompressible Reaction Zones

We first consider cases A and B. Sets of six OH fluorescence images for each of these two cases are included in Figs. 7 and 8. The images suggest that there are significant structural differences between the compressible and incompressible reacting shear layers, even though the convective Mach number for the compressible case is a modest 0.41. The images in Fig. 8 of the incompressible reaction zone, which has a convective Mach number of 0.11, are characterized by a few large patches of reacting or reacted fluid that are often linked by thin filamentary structures (flame sheets). These characteristics are reminiscent of the large-scale vortex and braid structures that have been well documented in low-speed planar mixing layers. The compressible reaction zone (Fig. 7) appears to be less organized, and the thin connecting structures or flame sheets are much less prominent. The qualitative differences between the compressible and incompressible reaction zones observed in the present work are analogous to the effects of compressibility on nonreacting shear layer structure reported by Clemens, et al.[7] and Clemens and Mungal.[17]

A second important difference between the incompressible and compressible cases is that the compressible reaction zone, as visualized by OH fluorescence, is narrower than its incompressible counterpart. This effect was quantified by obtaining average images of 150 shots and determining the widths of the average OH fluorescence profiles. Figure 9 shows profiles of the averaged fluorescence intensity for the two cases. These profiles were obtained by integrating the average images in the vertical direction over a narrow region ($\Delta x = 1$ mm) near the center of the image frame ($x = 38$ mm). The 10% intensity level is used to determine the visual width δ_{OH}, which is 5.9 mm for the compressible case and 8.7 mm for the incompressible case. These values are comparable to the widths calculated from Eqs. (3) and (4), which are 6.0 and 8.5 mm for cases A and B, respectively.

It is important to point out that for H_2-air combustion, in general, there is not necessarily a direct connection between the width obtained from OH images and the shear layer width determined from velocity measurements or sampling probe measurements of the mean scalar profile. This is because the reaction zone, where OH concentrations are high, is often separated from the high shear region of the mixing layer. As discussed earlier, we can expect OH fluorescence to be a reasonably good marker of the shear layer in the present study because the operating conditions of the burner can be selected to give an estimated equivalence ratio ϕ_s of the mixed fluid in the shear layer that is near the peak OH condition. This equivalence ratio is the same for both cases A and B ($\phi_s \cong 0.8$). Therefore, although the exact relationship between δ_{OH} and a velocity thickness (or conserved scalar thickness) is not known, the OH images provide useful information on shear layer growth and the relative widths for incompressible and compressible flows.

The results on visualized shear layer structure and thickness suggest that the effects of compressibility on the structure and growth rate of reacting shear layers are similar to the effects of compressibility on nonreacting shear layers. However, we must consider the possibility that the observed differences between cases A and B may be due, in part, to Reynolds number effects. Goebel and Dutton[32] reported that a fully developed state was not reached in their supersonic mixing

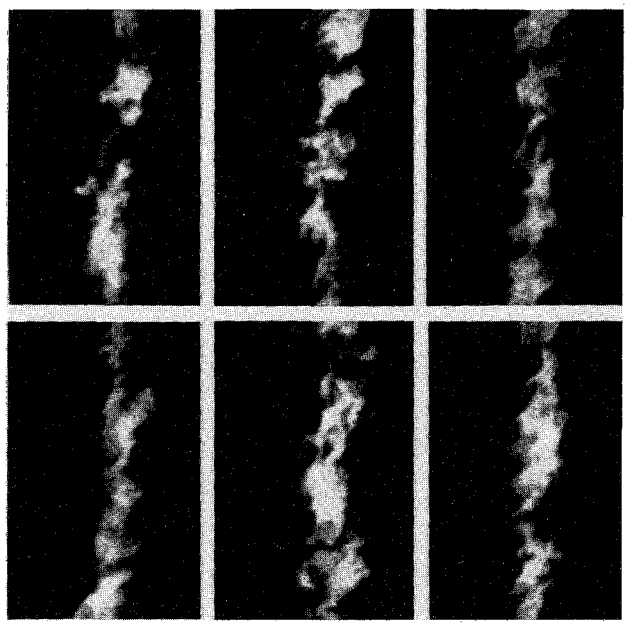

Fig. 7 OH fluorescence images from case A compressible reacting shear layer ($M_{c,1} = 0.41$). Location in the flow is shown in Fig. 6.

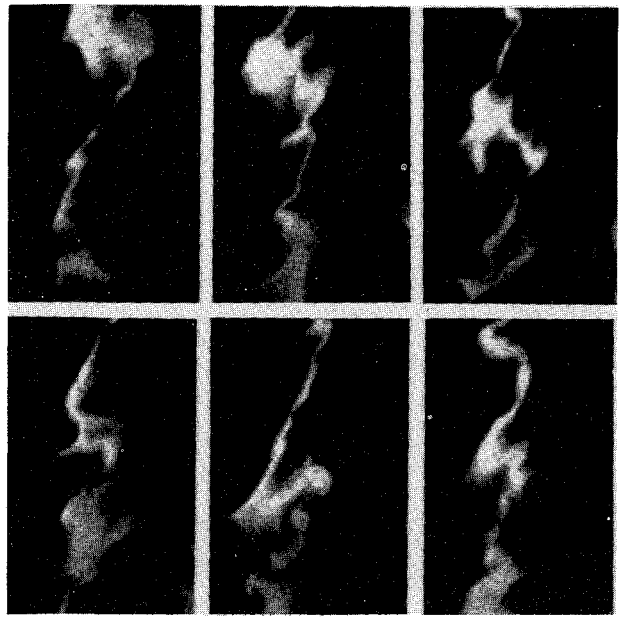

Fig. 8 OH fluorescence images from case B incompressible reacting shear layer ($M_{c,1} = 0.11$). Location in the flow is shown in Fig. 6.

layers until the local Reynolds number based on velocity thickness exceeded 100,000. The local Reynolds number listed in Table 1 for case A is 15,700. The Reynolds number for the incompressible case is only 6000 in the present study, and the shear layer observed in the near field of this flow may not have progressed sufficiently beyond the mixing transition to allow useful comparison with compressible flows at higher Reynolds numbers. Experiments that consider compressible and incompressible flows over a range of local Reynolds numbers that extends to higher values than those achieved in the present exploratory study will have to be conducted before conclusions can be drawn regarding the relative contributions of compressibility and Reynolds number effects to the observed differences between flames A and B.

Images (not included here) with the horizontal orientation of Fig. 6 show that the width of the core between the visualized reaction zones is typically 8–10 mm for the compressible case and that there is no consistent correlation (positive or negative) between structures on the two sides of the images.

Supersonic Lifted Flame

Images for case C are presented in Fig. 10 and show a reaction zone structure analogous to a lifted flame, but with the fuel on the outside of the jet rather than on the inside. The convective Mach number in this shear layer is nearly equal to that for case A (0.401 calculated for case C vs 0.413 for case A). The major difference between the flow conditions for the two cases is that the equivalence ratio of the low-speed stream has been increased from $\phi_2 = 5.0$ to $\phi_2 = 6.75$. The resulting change in the properties of the low-speed stream can affect the reacting shear layer in several ways. As shown in Fig. 2 and Table 1, the adiabatic flame temperature of the low-speed stream drops from 1400 K for case A to 1210 K for case C. Because the equilibrium concentrations of radicals are quite sensitive to temperature, one can expect the radical concentrations in the low-speed stream to decrease significantly with this drop in temperature. Radicals from the low-speed stream may contribute to the stability of the case A flame, and the reduction of radical concentrations in case C may lead to the observed lifted flame condition. The equivalence ratio of the mixed fluid in the compressible shear layer also changes. Our estimates show an increase from $\phi_s = 0.8$ to $\phi_s = 1.0$ going from the attached flame to the lifted flame, which suggests that the mixed fluid should be more reactive. However, the temperature of the mixed fluid (assuming no reaction between the unburned H_2 and the air) is lower for case C ($\sim$780 K) than for case A ($\sim$840 K).

The competition between turbulent mixing rates and chemical reaction rates can be characterized in terms of a Damköhler number,

$$Da = \tau_{\text{flow}}/\tau_{\text{chem}} \tag{8}$$

where τ_{flow} is a characteristic time scale for turbulent mixing, and τ_{chem} is a characteristic time scale for chemical reactions.

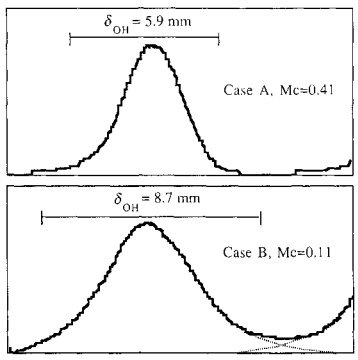

Fig. 9 Profiles of OH fluorescence intensity from averages of 150 images from cases A and B. Dashed lines approximate the overlapping profiles from each side of the annular shear layer.

Finite-rate chemistry effects are expected to become significant when the appropriately defined Damköhler number approaches unity. Previous studies[24,25] have used the large-eddy turnover time (or, equivalently, the inverse of the large-scale strain rate) to characterize turbulent mixing. In the present work the corresponding mixing time can be expressed as

$$\tau_{\text{flow}} = \sigma^{-1} = \frac{\delta}{(U_1 - U_2)} \tag{9}$$

where δ is the shear layer thickness from Eqs. (3) and (4). An appropriate chemical time scale for the consideration of extinction or liftoff phenomena in turbulent reacting flows is the residence time at the extinction limit for a perfectly stirred reactor (PSR) calculation. For the supersonic lifted flame shown in Fig. 10, the shear layer width δ was evaluated at $x = 38$ mm (the center of the image) to give a mixing time of $\tau_{\text{flow}} = 9.2$ μs. Chen[33] recently developed a PSR code that allows specification of two inlet streams, and this code was used to determine the extinction limit τ_{chem}. One of the PSR inlet streams was specified as air at the static temperature $T_1 = 493$ K, and the second inlet stream was specified as having the composition of the low-speed fluid, assuming adiabatic equilibrium and including radical concentrations. The flow ratio for the two streams was based on the shear layer entrainment ratio from Eq. (5), as listed in Table 1. The calculated residence time at extinction was $\tau_{\text{chem}} = 10$ μs. Hence, the Damköhler number calculated from the large-scale strain rate and the PSR extinction limit of the mixed fluid is near unity for the lifted flame in case C.

Both τ_{flow} and τ_{chem} are based on estimates; thus the result of $Da \cong 1$ for this lifted flame is somewhat fortuitous. Nevertheless, this result for the local Damköhler number in compressible reacting flows is consistent with the notion that the large-scale mixing time is the appropriate fluid dynamic time scale for characterizing turbulence-chemistry interactions in shear flows. An alternative would be to use the Kolmogorov time scale. However, scaling laws for fully developed turbulence give a $Re_\delta^{1/2}$ relationship between the large-scale mixing time and the Kolmogorov time scale. Therefore, a Damköhler number based on the Kolmogorov scale in this $Re_\delta = 17{,}900$ flow would be approximately 7×10^{-3}, which would suggest inappropriately that mixing times are two orders of magnitude faster than needed to produce significant turbulence-chemistry interactions. Experiments on incompressible reacting

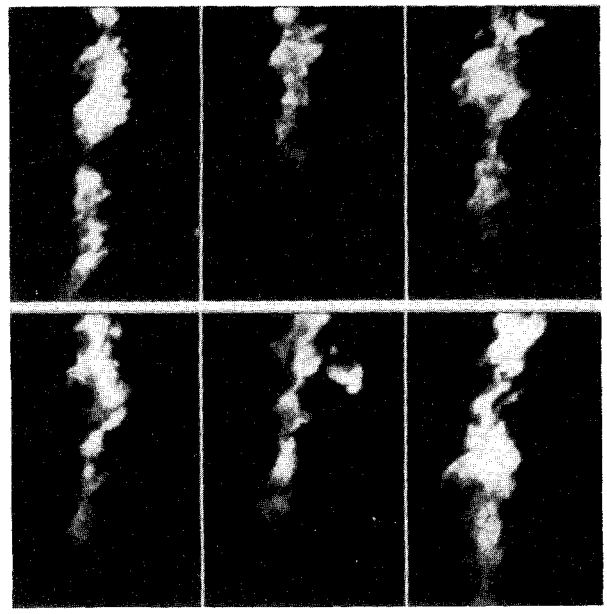

Fig. 10 OH fluorescence images from the case C compressible "lifted" flame ($M_{c,1} = 0.40$; $Da \cong 1$). Location in the flow is shown in Fig. 6.

flows[24,25] support the same conclusion regarding the use of the large-scale mixing time in forming the Damköhler number.

This result of a near-unity local Damköhler number is intriguing because it suggests the possibility of predicting the regimes of stable combustion in compressible reacting flows by combining correlations from nonreacting flows with relatively simple PSR calculations. The situation is not so simple, since the Damköhler number calculated for the stable attached flame in case A is also near unity. The large-scale mixing times are nearly equal for cases A and C, and the PSR extinction limit for case A is 9 μs, which is not significantly lower than the 10 μs calculated for case C. The implicit assumption in the simple formulation of the Damköhler number used here is that the shear layer can be treated as a homogeneous reactor. The fact that the estimates of the Damköhler are near unity for both the lifted and the attached flame suggests that this simple model is useful but is not complete. The stability of a reacting shear layer, with respect to liftoff and blowout, is expected to depend on freestream conditions and conditions in the flamesheets at the boundaries of the shear layer, as well as conditions within the mixed fluid. (These comments regarding the approximate nature of the Damköhler number calculation apply equally to incompressible reacting flows.) Additional experiments will be required to investigate the importance of various parameters that affect the stability of compressible reacting shear layers in this axisymmetric geometry.

Reaction at the Boundary of an Underexpanded Jet

In supersonic cases A and C, the central jet was operated at the matched pressure condition to produce a flow that was free of strong shocks. Images of the reacting shear layer were also obtained for the case of an underexpanded central jet. This flow is of interest because the barrel shock structure of the underexpanded jet constitutes a perturbation of the reacting shear layer, and the identification of mechanisms that can enhance mixing rates in compressible reacting flows is an area of active research.

The supersonic burner was operated with an air stagnation pressure of 500 kPa and a stagnation temperature of 695 K to produce an underexpanded jet. (Ideal expansion to atmospheric pressure would produce a Mach 1.7 jet, whereas the nozzle design is for Mach 1.5.) The equivalence ratio ϕ_2 of the low-speed, flat-flame products was 5.0, the same as for cases A and B. A matched jet with these conditions would have an estimated convective Mach number of 0.44, slightly higher than for case A. However, because of the presence of shocks, the simple analysis to estimate shear layer properties cannot be applied to the underexpanded jet.

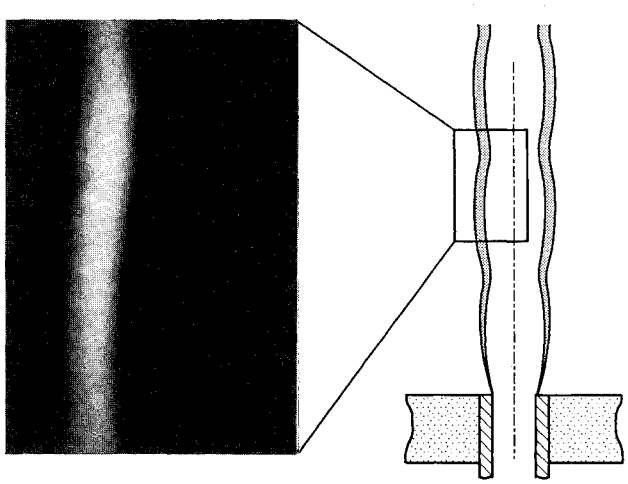

Fig. 11 Illustration of the observed cell structure of the reaction zone surrounding the underexpanded jet and the corresponding ensemble-averaged OH fluorescence image. The size and streamwise position of the image frame are the same as those in Fig. 6.

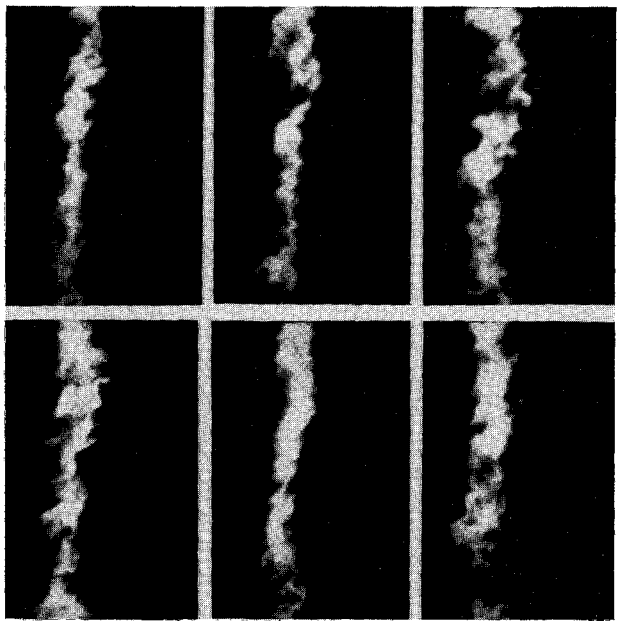

Fig. 12 OH fluorescence images from the underexpanded case.

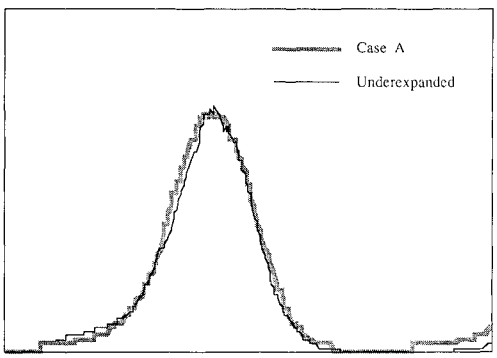

Fig. 13 Comparison of ensemble-averaged OH fluorescence profiles at $x = 38$ mm from the underexpanded and matched cases. (The underexpanded profile has been translated radially to align the peaks of the two profiles.)

With these operating conditions a stable, attached, supersonic flame was observed. The radius of the luminous reaction zone varied periodically, producing a visual appearance of cells, as illustrated in Fig. 11. This cell structure was visible over the full length of the luminous reaction zone, which extended as far downstream as 200 mm (~25 diam). Figure 11 includes an ensemble average of 150 frames which shows a reaction zone that bows out and back in through a gradual curve, then quickly bends out again to repeat the pattern. This periodic deflection of the reacting shear layer, which results from the interaction of the reaction zone with the barrel shock structure of the underexpanded jet, does not have a significant effect on the large-scale turbulence structure or the spreading rate. The instantaneous images in Fig. 12 reveal a turbulence structure similar to that for case A (compare Fig. 7). Figure 13 compares profiles of the average fluorescence intensity in the underexpanded and matched cases and shows that the visualized reaction zone widths are the same.

Summary and Conclusions

We have described an axisymmetric burner for investigations of the effects of convective the Mach number, the Reynolds number, and the Damköhler number on the structure, growth rate, and stability of reacting turbulent shear layers. In this relatively simple facility, a central freejet of resistively heated air is surrounded by a low-speed co-flow of fuel-rich

products from a H_2-air flat flame. An annular reacting turbulent shear layer is formed in the near field of the air jet as the hydrogen-rich products are entrained. The ranges of operating parameters for this burner were analyzed, based on theories and correlations for nonreacting compressible flows. This analysis showed that the present facility can be used to investigate the effects of compressibility up to a convective Mach number of ~0.54 using air as the central jet and 0.80 using 20% oxygen in helium. Analysis also showed that this burner can be operated to give an equivalence ratio for the mixed fluid in the shear layer that is near unity. Consequently, heat release occurs within the shear layer (rather that at its edge), and OH fluorescence can be expected to be a good qualitative marker of the fluid in the reacting shear layer. Results of OH fluorescence imaging experiments were presented for 1) an attached compressible flame, 2) an attached incompressible flame, 3) a lifted compressible flame, and 4) a flame at the boundary of an underexpanded jet. Comparison of the two attached flames suggests that compressibility affects reacting and nonreacting shear layers in similar ways; the growth rate is reduced, and the organization of visualized structures into large-scale regions (order of the shear layer thickness) connected by thin "braids" or "flame sheets" becomes less prominent as the convective Mach number increases. The Reynolds numbers for these initial experiments were relatively low, and additional experiments at higher Reynolds numbers will have to be conducted before firm conclusions may be drawn.

The Damköhler number, based on the local large-scale strain rate in the shear layer and the extinction limit for a perfectly stirred reactor calculation, was near unity for the lifted compressible flame. This suggests that the large-scale strain rate rather than the strain rate at the Kolmogorov scale is the appropriate one to use in characterizing extinction phenomena in compressible reacting flows, a result that is in agreement with earlier results for incompressible reacting flows.

Periodic deflection of the reaction zone by the barrel shock structure of an underexpanded jet did not produce significant observable changes in the large-scale turbulence structure or the width of the compressible reacting shear layer.

Acknowledgments

This work was supported by the United States Department of Energy through Sandia's Exploratory Research and Development program and through the DOE Office of Basic Energy Sciences, Division of Chemical Sciences. The authors thank Prof. J.-Y. Chen for providing the PSR results used in this paper. Drs. J. H. Chen and N. T. Clemens provided many useful insights on the structure of nonreacting compressible layers. The technical contributions of T. Prast, M. Kimmel, and G. Sartor are gratefully acknowledged.

References

[1]Dimotakis, P., "Turbulent Free Shear Layer Mixing," AIAA Paper 89-0262, Jan. 1989.

[2]Papamoschou, D., and Roshko, A., "The Compressible Turbulent Shear Layer: An Experimental Study," *Journal of Fluid Mechanics,* Vol. 197, 1988, pp. 453–477.

[3]Papamoschou, D., "Structure of the Compressible Turbulent Shear Layer," *AIAA Journal,* Vol. 29, 1991, pp. 680–691.

[4]Chinzei, N., Masuya, G., Komuro, T., Murakami, A., and Kudou, K., "Spreading of Two-Stream Supersonic Turbulent Mixing Layers," *Physics of Fluids,* Vol. 29, 1986, pp. 1345–1347.

[5]Samimy, M., and Elliot, G. S., "Effects of Compressibility on the Structure of Free Shear Layers," AIAA Paper 88-3054, July 1988.

[6] Shau, Y. R., and Dolling, D. S., "Experimental Study of Spreading Rate Enhancement of High Mach Number Turbulent Shear Layers," AIAA Paper 89-2458, Jan. 1989.

[7]Clemens, N. T., Mungal, M. G., Berger, T. E., and Vansburger, U., "Visualization of the Structure of the Turbulent Mixing Layer Under Compressible Conditions," AIAA Paper 90-0500, Jan. 1990.

[8]Bogdanoff, D. W., "Compressibility Effects in Turbulent Shear Layers," *AIAA Journal,* Vol. 21, No. 6, 1983, pp. 926–927.

[9]Ikawa, H., Kubota, T., "Investigation of Supersonic Turbulent Mixing Layer with Zero Pressure Gradient," *AIAA Journal,* Vol. 13, No. 5, 1975, pp. 566–572.

[10]Ragab, S. A., and Wu, J. L., "Linear Instabilities in Two-Dimensional Compressible Mixing Layers," *Physics of Fluids A,* Vol. 1, 1989, pp. 957–966.

[11]Zhuang, M., Kubota, T., and Dimotakis, P. E., "On the Stability of Inviscid, Compressible Free Shear Layers," *First National Fluid Dynamics Conference,* Vol. II, 1988, pp. 768–773.

[12]Sandham, N. D., and Reynolds, W. C., "The Compressible Mixing Layer: Linear Theory and Direct Simulation," AIAA Paper 89-0371, Jan. 1989.

[13]Brown, G. L., and Roshko, A., "On Density Effects and Large Structure in Turbulent Mixing Layers," *Journal of Fluid Mechanics,* Vol. 64, 1974, pp. 775–816.

[14]Sandham, N. D., and Reynolds, W. C., "Three-Dimensional Simulation of Large Eddies in the Compressible Mixing Layer," *Journal of Fluid Mechanics,* Vol. 224, 1991, pp. 133–158.

[15]Chen, J. H., "The Effect of Compressibility on Conserved Scalar Mixing in a Plane Free Shear Layer," Eighth Turbulent Shear Flows Symposium, Paper 9-4, Munich, Germany, Sept. 1991.

[16]Fourguette, D. C., Mungal, M. G., and Dibble, R.W., "Time Evolution of the Shear Layer of a Supersonic Axisymmetric Jet at Matched Conditions," *AIAA Journal,* Vol. 27, No. 8, 1991, pp. 1123–1130.

[17]Clemens, N. T., and Mungal, M. G., "Two- and Three-Dimensional Effects in the Supersonic Mixing Layer," AIAA Paper 90-1978, July 1990; also *AIAA Journal,* Vol. 30, No. 4, 1992, pp. 973–981.

[18]Wallace, A. K., "Experimental Investigation on the Effects of Chemical Heat Release in the Reacting Turbulent Plane Shear Layer," Ph.D. Dissertation, Univ. of Adelaide, Adelaide, Australia, 1981; see also AFOSR-TR-84-0650.

[19]Hermanson, J. C., and Dimotakis, P. E., *Journal of Fluid Mechanics,* Vol. 199, 1989, pp. 513–553.

[20]McMurtry, P. A., Jou, W. H., Riley, J., and Metcalfe, R. W., *AIAA Journal,* Vol. 24, No. 6, 1986, pp. 962–970.

[21]McMurtry, P. A., and Riley, J. , "Mechanisms by which Heat Release Affects the Flow Field in a Chemically Reacting Turbulent Mixing Layer," AIAA Paper 87-0131, Jan. 1987.

[22]Shin, D. S., and Ferziger, J. H. "Stability of Compressible Reacting Mixing Layer," AIAA Paper 91-0372, Jan. 1991.

[23]Magre, P., and Dibble, R. W., "Turbulent Diffusion Flames," *Combustion and Flame,* Vol. 73, 1988, pp. 195–206.

[24]Barlow, R. S., Dibble, R. W., Chen, J.-Y., and Lucht, R. P., "Effect of Damköhler Number on Superequilibrium OH Concentration in Turbulent Nonpremixed Jet Flames," *Combustion and Flame,* Vol. 82, 1990, pp. 235–251.

[25]Mungal, M. G., and Frieler, C. E., "The Effects of Damköhler Number in a Turbulent Shear Layer," *Combustion and Flame,* Vol. 71, 1988, pp. 23–34.

[26]Kerstein, A. R., "Linear-Eddy Modeling of Turbulent Transport. II: Application to Shear Layer Mixing," *Combustion and Flame,* Vol. 75, 1989, pp. 397–413.

[27]Barlow, R. S., Dibble, R. W., and Fourguette, D. C., "Departure from Chemical Equilibrium in a Lifted Hydrogen Flame," AIAA Paper 89-2523, July 1989.

[28]Yip, B., Lyons, K., Long, M., Mungal, M. G., Barlow, R. S., and Dibble, R. W., "Visualization of a Supersonic Underexpanded Jet by Planar Laser Rayleigh Scattering," *Physics of Fluids A,* Vol. 1, 1990, p. 1449.

[29]Tam, C. K. W., and Hu, F. Q., "On the Three Families of Instability Waves of High-Speed Jets," *Journal of Fluid Mechanics,* Vol. 201, 1989, pp. 447–483.

[30]Samimy, M., Zaman, K. B. M. Q., and Reeder, M. F., "Supersonic Jet Mixing Enhancement by Vortex Generators," AIAA Paper 91-2263, June, 1991.

[31]Long, M. B., "IMP Software for Ditgital Image Acquisition and Processing on the Mac II Computer."

[32]Goebel, S. G., and Dutton, J. C., "Velocity Measurements of Compressible, Turbulent Mixing Layers," AIAA Paper 90-0709, Jan. 1990.

[33]Chen, J.-Y., Sandia National Labs., Personal Communication, 1991.